Emerging Materials Research
Volume 2 Issue EMR4
Synthesis and magnetic properties of fergusonite-structured La(NbVMn)O_4
Kawakami *et al.*

ice | science

Pages 191–197 http://dx.doi.org/10.1680/emr.13.00018
Research Article
Received 13/05/2013 Accepted 05/08/2013
Published online 09/08/2013
Keywords: bulk materials/defects/electronic structure of atoms and molecules/magnetic properties

ice Institution of Civil Engineers
publishing

Synthesis and magnetic properties of fergusonite-structured La(NbVMn)O_4

Shunsuke Kawakami MEng
Department of Materials Science, Kyushu Institute of Technology, Kitakyushu, Japan

Naoya Takeda MEng
Department of Materials Science, Kyushu Institute of Technology, Kitakyushu, Japan

Shigemi Kohiki Dr. Eng.*
Department of Materials Science, Kyushu Institute of Technology, Kitakyushu, Japan

Fuki Tsutsui MEng
Department of Materials Science, Kyushu Institute of Technology, Kitakyushu, Japan

Juri Harada BEng
Department of Materials Science, Kyushu Institute of Technology, Kitakyushu, Japan

Masao Arai Dr. Eng.
National Institute for Materials Science, Tsukuba, Japan

Masanori Mitome Dr. Sci.
National Institute for Materials Science, Tsukuba, Japan

Kazuyo Ohmura MEng
Institute for Materials Research, Tohoku University, Sendai, Japan

Kunio Yubuta Dr. Eng.
Institute for Materials Research, Tohoku University, Sendai, Japan

Toetsu Shishido Dr. Eng.
Institute for Materials Research, Tohoku University, Sendai, Japan

The authors have synthesized fergusonite-structured La($Nb_{0.71}V_{0.04}Mn_{0.25}$)$O_4$ samples. The samples, consisting of La^{3+}, Nb^{5+}, V^{5+}, Mn^{4+} and oxygen ions, demonstrated temperature-dependent magnetization that increased with lowering the temperature below ≈200 K, and almost saturated below ≈100 K. At 75 K, the field-dependent magnetization demonstrated sigmoidal curve and reached 3 μ_B/Mn at 1 T. Such a magnetic behavior can be ascribed to exchange interaction between $Mn^{4+}Nb_2O_{11}$ nanoclusters. The Mn^{4+} substitution for the V^{5+} sites of the crystal resulted also in the occupied state above the valence band maximum.

1. Introduction

Multiferroics, in which ferromagnetic (FM) or anti-FM, ferroelectric and ferroelastic order parameters coexist, attract a great attention for the development of multifunctional devices.[1] Lanthanum orthoniobate, $LaNbO_4$, and acceptor-doped $LaNbO_4$ are of great interest, respectively, for their potential in functional device applications[2–6] and for high proton conductivity in solid fuel cell applications.[7,8] $LaNbO_4$ crystal has two polymorphs: the scheelite structure with tetragonal symmetry (space group $I4_1/a$) and the fergusonite structure with monoclinic symmetry (space group $I2/c$). Below 770 K, the crystal transforms from the scheelite into the fergusonite structure. The phase transition is associated with stress-induced ferroelasticity.[1] When the fergusonite crystal acquires FM functionality, ferroelasticity is advantageous for the development of pressure-sensitive nonvolatile memory.

$La(Nb_{0.7}V_{0.3})O_4$ is an analogue of $LaNbO_4$ with tetrahedral moieties,[9,10] in which V^{5+} ions substitute randomly for the Nb^{5+} sites of $LaNbO_4$, and crystallizes into the scheelite structure at room temperature (RT).[10] It is known that the solution energy with doping depends on the ionic radii (r_{ion}). Although r_{ion} of tetrahedrally coordinated V^{5+} (0·036 nm) is smaller than that of tetrahedrally coordinated Nb^{5+} (0·048 nm),[11] V^{5+} ions substitutes readily for Nb^{5+} ions since V and Nb belong to the same group in the periodic table. However, for *d*-block elements such as V and Mn, chemical similarities in the horizontal of the table can be more important than the vertical one, and r_{ion} of tetrahedrally coordinated V^{5+} is similar to that of tetrahedrally coordinated Mn^{4+} (0·039 nm).[11] Accordingly, we expect that Mn^{4+} (d^3) ions substitute for the V^{5+} (d^0) sites of $La(Nb_{0.7}V_{0.3})O_4$, and the substitution generates oxygen vacancy (V_O) for maintaining electrical neutrality.

As a first step to FM and ferroelastic functional material, the authors attempted to dope Mn^{4+} to $La(Nb_{0.7}V_{0.3})O_4$. The fergusonite-structured Mn-doped $La(NbV)O_4$ sample, exhibiting FM behavior based on magnetic nanoclusters, was successfully synthesized. X-ray photoemission spectroscopy (XPS) clarified the Mn^{4+}, V^{5+} and Nb^{5+} chemical states for floating zone (FZ)-treated Mn-doped $La(NbV)O_4$. On the basis of condensation of NbO_4 tetrahedra and formation of $[Nb_3O_{11}]^{7-}$ or $[Nb_2O_7]^{4-}$ nanoclusters,[12,13] the observed magnetization M ≈3 μ_B/Mn at 75 K of the sample can be ascribed

*Corresponding author e-mail address: kohiki@che.kyutech.ac.jp

to $Mn^{4+}(d^3)Nb_2O_{11}$ nanoclusters generated by Mn^{4+} substitution for the tetrahedral V^{5+} sites of diamagnetic $La(NbV)O_4$ crystal.

2. Experiment

For synthesizing $La(Nb_{1-x}V_x)O_4$ samples, La_2O_3 (>99·95% purity, Kanto Chemical, Japan), Nb_2O_5 (>99·9% purity, Kojundo Chemical, Japan) and V_2O_3 (>99·9% purity, Kojundo Chemical) powders were weighed with the molar ratio of La:Nb:V = 1:1 − *x*:*x*, and then, the powders were mixed in grinding; subsequently, mixtures were heated at 1573 K in flowing oxygen gas for 4 h. X-ray diffraction (XRD) patterns at RT of $La(Nb_{1-x}V_x)O_4$ polycrystals were recorded by using a Rigaku (Japan) CN2013 diffractometer with Cu *K*α radiation. Since the sample with the nominal composition of $x = 0{\cdot}4$ demonstrated the most clearly single-phase XRD pattern of the scheelite structure as will be shown later, the authors substituted Mn for V of the $x = 0{\cdot}4$ samples. The powders of La_2O_3, Nb_2O_5, V_2O_3 and MnO_2 (>99·5% purity, Wako Pure Chemical, Japan), weighed with the molar ratio of La:Nb:V:Mn = 1:0·6:0·4 – *y*:*y* ($y = 0$, 0·1, 0·2 and 0·3), were mixed in grinding, and subsequently heated at 1573 K in flowing oxygen gas for 4 h. As shown later, the $La(Nb_{0\cdot6}V_{0\cdot4-y}Mn_y)O_4$ samples, with $y = 0{\cdot}3$, showed clearly single-phase XRD pattern of the fergusonite structure. Polycrystals with the nominal composition of $La(Nb_{0\cdot6}V_{0\cdot1}Mn_{0\cdot3})O_4$ were pulverized, and the resulting powders were pressed into a rod with a diameter of ≈5 mm and a length of ≈100 mm and sintered again at 1350 K for 30 h in air. A SS35WV double hemi-ellipsoid halogen-lamp image furnace (ASGAL Co., Japan) was used for FZ treatment of the $La(Nb_{0\cdot6}V_{0\cdot1}Mn_{0\cdot3})O_4$ rod in flowing oxygen gas at a growth rate of 30 mm/h with simultaneous rotation of feed and seed rods at 20 rpm in opposite directions. The FZ-treated section had typical diameter of ≈5 mm and length of ≈30 mm. A thin platelet-like sample was cut from the treated section across the major axis of the rod for XPS using a Shimadzu-Kratos (Japan) AXIS-Ultra DLD spectrometer with monochromatized Al *K*α radiation in a vacuum pressure less than 2×10^{-10} Torr. The spectrometer was calibrated by the Au $4f_{7/2}$ (84·0 eV) electrons. To stabilize the spectra and compensate charging, the sample surface was flooded with low-energy electrons from a neutralizer. The estimated electron energy uncertainty was ±0·15 eV. Temperature and field dependences of magnetization (*M*-*T* and *M*-*H*) for the sample with the nominal composition of $La(Nb_{0\cdot6}V_{0\cdot1}Mn_{0\cdot3})O_4$ were examined by using a Quantum Design (USA) MPMS-5S superconducting quantum interference devise magnetometer. For *M*-*T* measurements, the sample was cooled to 5 K without *H*, and then *H* was applied for zero-field-cooled (ZFC) measurements. ZFC magnetization was recorded with rising temperature up to 300 K. After the ZFC measurements, the sample was cooled again to 5 K in the same *H*, and then field-cooled (FC) magnetization was recorded with rising temperature to 300 K.

3. Results and discussion

As shown in Figure 1(a), $La(Nb_{1-x}V_x)O_4$ polycrystals indicated gradual change in crystal structure from the fergusonite $LaNbO_4$ with $a = 0{\cdot}556$, $b = 1{\cdot}156$, $c = 0{\cdot}522$ nm and $\beta = 94{\cdot}0^\circ$ (JCPDS 22-1125) at $x = 0$ to scheelite $La(Nb_{0\cdot7}V_{0\cdot3})O_4$ with $a = 0{\cdot}534$ and $b = 1{\cdot}172$ nm (ICDD 04-010-2132) at $x = 0{\cdot}4$. As mentioned before, the diffraction pattern of the scheelite structure was most clear for the $x = 0{\cdot}4$ sample. The scheelite $La(Nb_{0\cdot7}V_{0\cdot3})O_4$ remained as the major phase for $x = 0{\cdot}6$; however, the fergusonite $LaVO_4$ (JCPDS 23-0324) also appeared above $x = 0{\cdot}5$. The $LaVO_4$ grew significantly with $x \geq 0{\cdot}5$, but La_2VO_7 (ICDD 00-037-0078) was also observed at $x = 1$ beside the major $LaVO_4$. The vapor pressure of V_2O_3 must be higher than those of refractory La_2O_3 and Nb_2O_5, so the V_2O_3-rich mixture at $x = 0{\cdot}4$ resulted in the scheelite $La(Nb_{0\cdot7}V_{0\cdot3})O_4$ crystal after heat treatment at 1573 K in flowing oxygen gas for 4 h. As shown by Figure 1(b), the crystal structure of $La(Nb_{0\cdot6}V_{0\cdot4-y}Mn_y)O_4$ varied with increasing *y* from the scheelite to the fergusonite structure. Polycrystals with the nominal composition of $La(Nb_{0\cdot6}V_{0\cdot1}Mn_{0\cdot3})O_4$ demonstrated clearly single-phase XRD pattern of the fergusonite structure. Mn ions substituted for the V sites lowered symmetry of the crystal at RT to monoclinic peculiar to ferroelasticity.

As seen in Figure 2(a), the FZ treatment for the $La(Nb_{0\cdot6}V_{0\cdot1}Mn_{0\cdot3})O_4$ rod gave rise to the (–121) preferred orientation growth of the fergusonite structure across the major axis of the rod. A thin platelet-like sample was cut from the treated section of the rod, and then the cut plane of the platelet-like $La(Nb_{0\cdot6}V_{0\cdot1}Mn_{0\cdot3})O_4$ sample was provided for XPS. From the intensity of the La $3d_{5/2}$, Nb $3d_{5/2}$, V $2p_{3/2}$, and Mn $2p_{3/2}$ peaks (Figure 2(b)) and the relative sensitivity factors,[14] the atomic ratio of the sample was estimated to be La:Nb:V:Mn = 1:0·75:0·04:0·21. Semi-quantitatively determined composition of the sample, by XPS, can be expressed as $La(Nb_{0\cdot75}V_{0\cdot04}Mn_{0\cdot21})O_4$. The binding energy ($E_B$) of the La $3d_{5/2}$, Nb $3d_{5/2}$, V $2p_{3/2}$, and Mn $2p_{3/2}$ electrons were 834·9, 207·3, 517·8 and 641·9 eV, respectively. These E_Bs correspond to those of La_2O_3, Nb_2O_5, V_2O_5 and MnO_2, respectively.[14] The chemical state of the constituents can be assigned as La^{3+}, Nb^{5+}, V^{5+} and Mn^{4+}. Thus, the tetrahedral V^{5+} sites of diamagnetic $La(NbV)O_4$ crystal were substituted by Mn^{4+} ions. Therefore, the $La(Nb_{0\cdot71}V_{0\cdot04}Mn_{0\cdot25})O_4$ sample is expected to bring about *M* of 3 μ_B/Mn.

As seen in Figure 3(a), the $La(Nb_{0\cdot71}V_{0\cdot04}Mn_{0\cdot25})O_4$ sample exhibited FM behavior in *M*-*T*, while the reference sample, nominally $La(Nb_{0\cdot6}V_{0\cdot4})O_4$, was diamagnetic. FC and ZFC magnetizations in *M*-*T* for the $La(Nb_{0\cdot71}V_{0\cdot04}Mn_{0\cdot25})O_4$ samples agreed with each other for $H = 0{\cdot}5$ T. The Curie temperature of ≈200 K was derived from (1/*M*)-*T* plot. As shown in Figure 3(b), the $La(Nb_{0\cdot71}V_{0\cdot04}Mn_{0\cdot25})O_4$ sample demonstrated sigmoidal *M*-*H* curve even at 200 K. At 75 K, *M* for a Mn ion almost saturated above $H = 0{\cdot}5$ T, and then reached 3 μ_B at $H = 1$ T. The sigmoidal *M*-*H* curve, growing larger with lowering the temperature, is consistent with the *M*-*T* curve mentioned above. As shown in Figure 3(c), the initial magnetization curve at 75 K fitted well with the Langevin function $M = N\mu(\coth(\mu H/k_BT) - (k_BT/\mu H))$, where *N* is the number of the magnetic moment μ per unit volume and k_B is the Boltzmann constant. When $\mu = 3\ \mu_B$ was assumed for a Mn^{4+} ion ($S = 3/2$, $g = 2$), $N = 600$ was obtained. Although no bifurcation was seen between curves of the initial magnetization

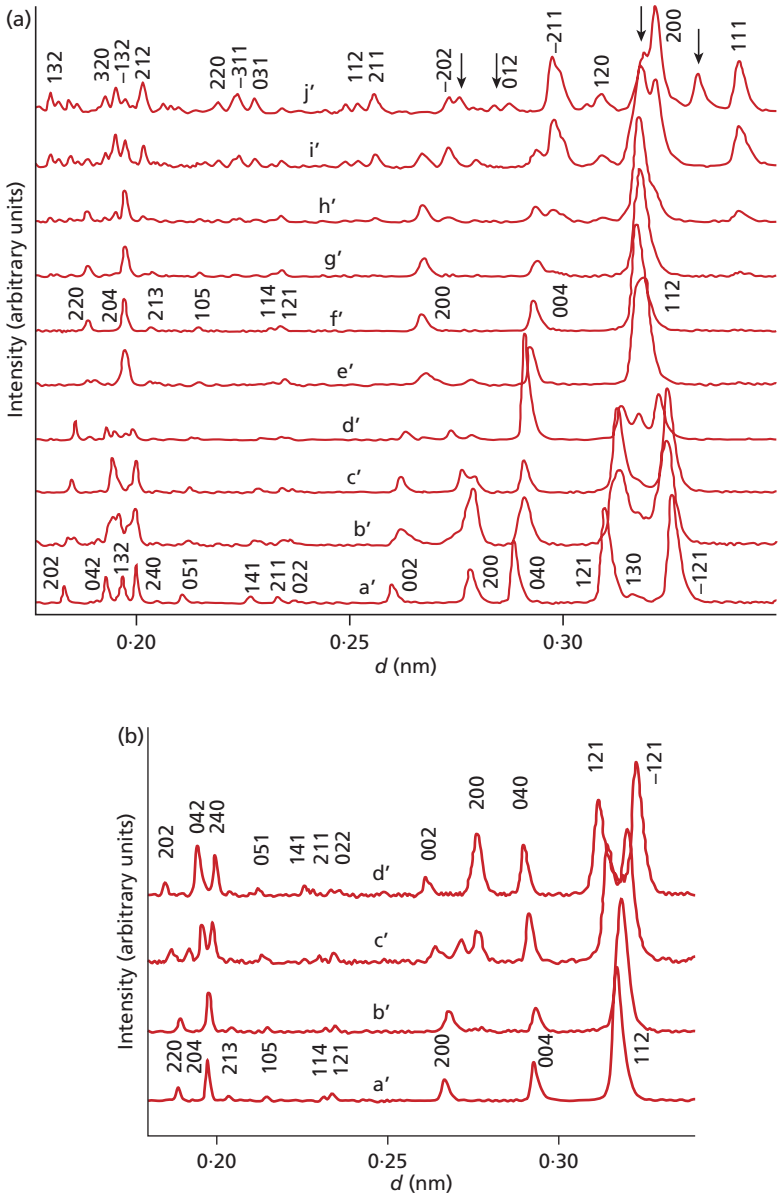

Figure 1. (a) X-ray diffraction pattern of the $La(Nb_{1-x}V_x)O_4$ samples with the nominal composition x = 0 (a′), 0·05 (b′), 0·1 (c′), 0·2 (d′), 0·3 (e′) 0·4 (f′), 0·5 (g′), 0·6 (h′), 0·8 (i′) and 1 (j′). The inter-plane space d was derived from the diffraction angle θ by $\lambda = 2d\sin\theta$ with λ = 0·154184 nm. Arrows in the pattern (j′) correspond possibly to La_2VO_7 (ICDD 00-037-0078). (b) X-ray diffraction pattern of the $La(Nb_{0·6}V_{0·4-y}Mn_y)O_4$ samples with the nominal composition y = 0 (a), 0·1 (b), 0·2 (c) and 0·3 (d).

(A) and the Langevin function (B) below H = 0·25 T, the difference (A – B) increased as H increased above H = 0·25 T. The difference (A – B), and also the *M-T* and *M-H* curves suggest that the observed FM behavior originates from growth in distance of exchange interactions between dispersed magnetic nanoclusters containing Mn^{4+} (3 μ_B) ions with lowering temperature.[15]

On the scheelite $LaNbO_4$ crystal, the energetic features of V_O by atomistic simulation[12] and total energy calculations of V_O[13] were reported. Significant relaxation of NbO_4 tetrahedra around V_O resulted in the formation of an $[Nb_2O_7]^{4-}$ group, which is facilitated by the rotation of the nearer of the two $[NbO_4]^{3-}$ tetrahedra. Condensation of two or three NbO_4 units formed an $[Nb_2O_7]^{4-}$ or $[Nb_3O_{11}]^{7-}$ group.

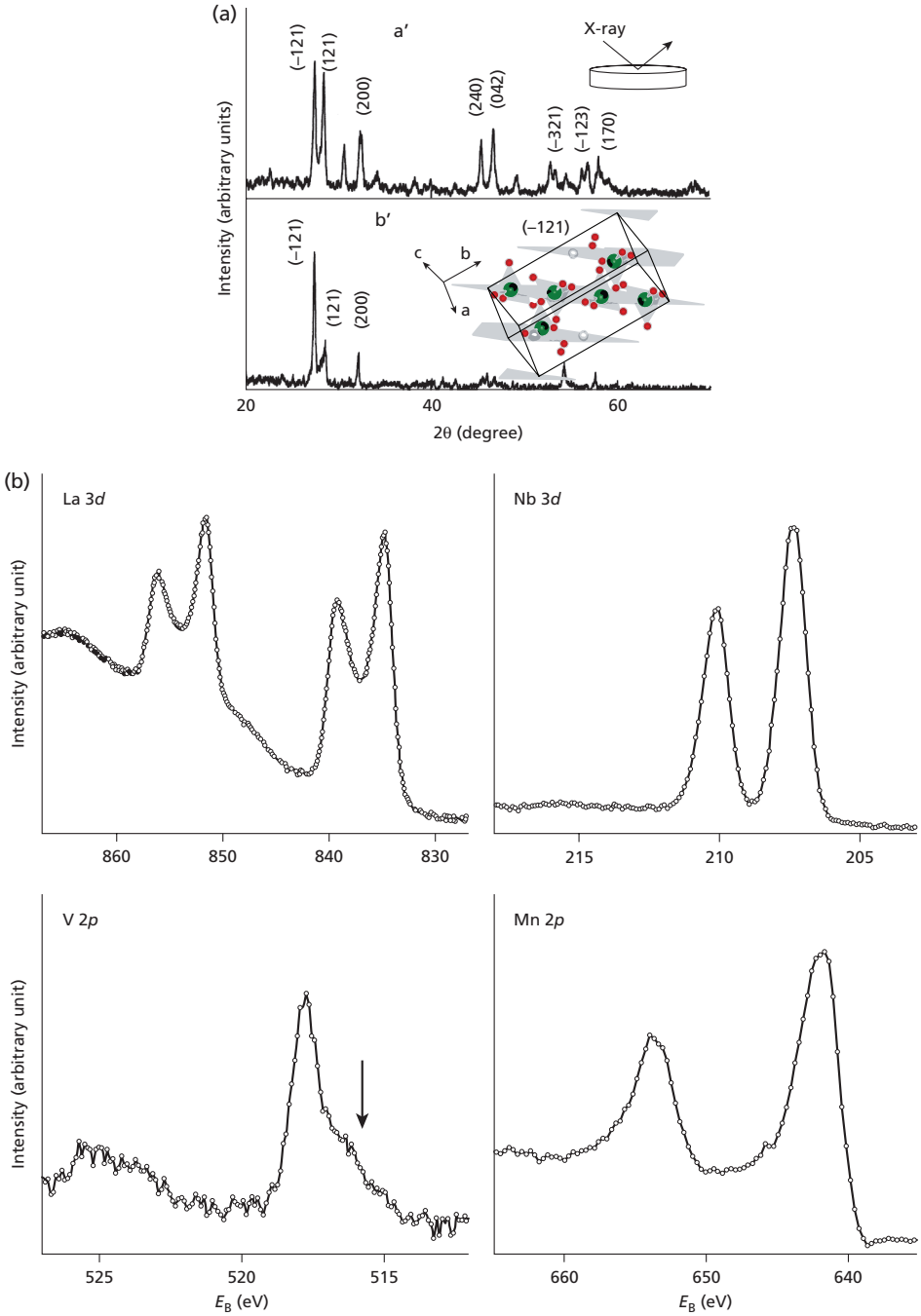

Figure 2. (a) X-ray diffraction patterns before (a′) and after (b′) the FZ treatment. Insets of (a′) and (b′) are illustrations of the platelet-like sample cut across the major axis of the rod, and of the (–121) plane of the fergusonite $LaNbO_4$, respectively. (b) La 3*d*, Nb 3*d*, V 2*p* and Mn 2*p* spectra of the sample. An arrow in the V $2p_{3/2}$ spectrum pointing to a peak shoulder suggests coexistence of the V^{4+} state as a minor component.

Thus, tetrahedrally coordinated V^{5+} sites are expected to lose oxygen by Mn^{4+} substitution. In the case of a neutral $V_O^{\times}$, the MnO_4 coordination tetrahedron loses one vertex and becomes triangular, while positively ionized $V_O^{\cdot\cdot}$ and $V_O^{\cdot}$ cause significant perturbation of the surrounding

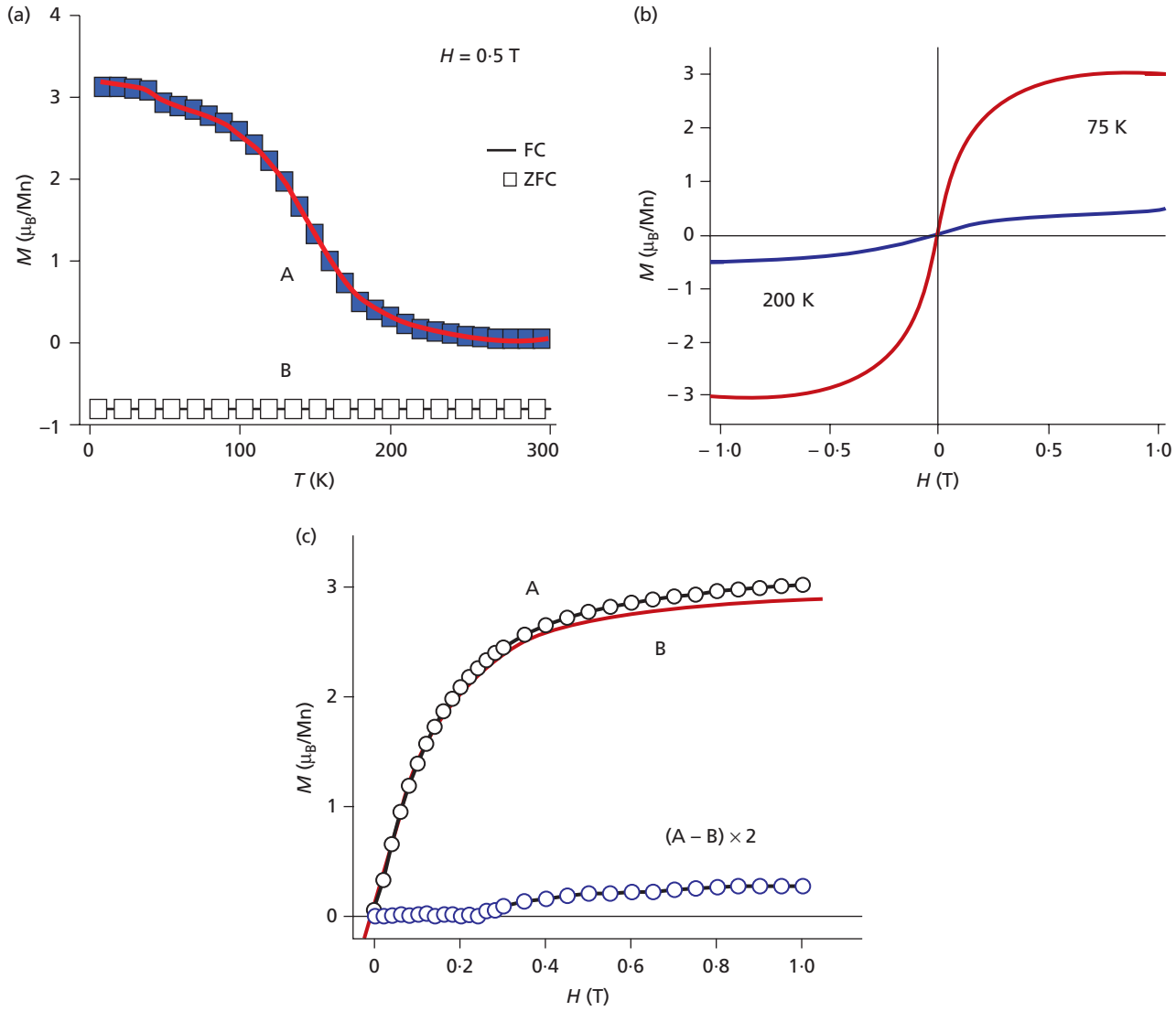

Figure 3. (a) *M-T* curves of the $La(Nb_{0·75}V_{0·04}Mn_{0·21})O_4$ sample (A) and a reference with nominal composition $La(Nb_{0·6}V_{0·4})O_4$ (B) in $H = 0·5$ T. Slightly enlarged *M* below 43 K of the sample (A) may be due to Mn_3O_4 nanoparticles residing in the sample. (b) *M-H* curves of the $La(Nb_{0·75}V_{0·04}Mn_{0·21})O_4$ sample at 75 and 200 K. (c) fitting of the initial magnetization curve (A) to the Langevin function (B). Curve (A – B) indicates difference between A and B.

lattice[12,13]. Reconstruction around $V_O^{\cdot\cdot}$ and $V_O^{\cdot}$ are expected to form $Mn^{4+}Nb^{5+}{}_2O_{11}$ and $Mn^{4+}Nb^{5+}O_7$ structures, respectively, linked by sharing a corner oxygen, as illustrated in Figure 4. The magnetic moment for $V_O^{\cdot\cdot}$ and $V_O^{\cdot}$ are 0 and 1 μ_B, respectively. Therefore, $M = 3$ μ_B/Mn observed for the $La(Nb_{0·71}V_{0·04}Mn_{0·25})O_4$ sample is ascribable to the exchange interaction between $Mn^{4+}Nb_2O_{11}$ nanoclusters.

Aforementioned Mn^{4+} substitution for the V^{5+} site is antcipated resulting in a hump above the valence band maximum (VBM). Figure 5(a) shows the density of states (DOS) for $LaNbO_4$ with the fergusonite crystal structure calculated by using the generalized-gradient approximation (GGA) to density functional theory[15] under the conditions reported in detail elsewhere.[5] The VB constructed mostly from O 2*p* orbitals distributes from 5 to 0 eV below VBM. VB showed complex dispersions, which reflected oxygen sites (O_1 and O_2), split into two structurally inequivalent positions in the fergusonite crystal structure. The calculated DOS showed a three-peaked structure. The one is originated from O_2, the other one is from

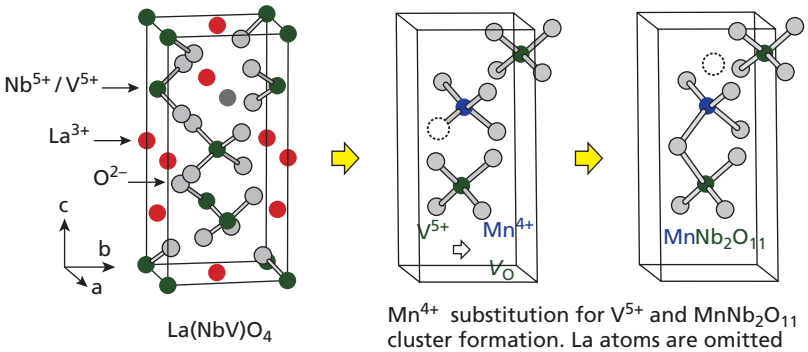

Figure 4. Schematic of oxygen loss by Mn^{4+} substitution for tetrahedrally coordinated V^{5+} sites and reconstruction around $V_O^{\cdot\cdot}$ forming $Mn^{4+}Nb^{5+}{}_2O_{11}$ structure linked by sharing a corner oxygen.

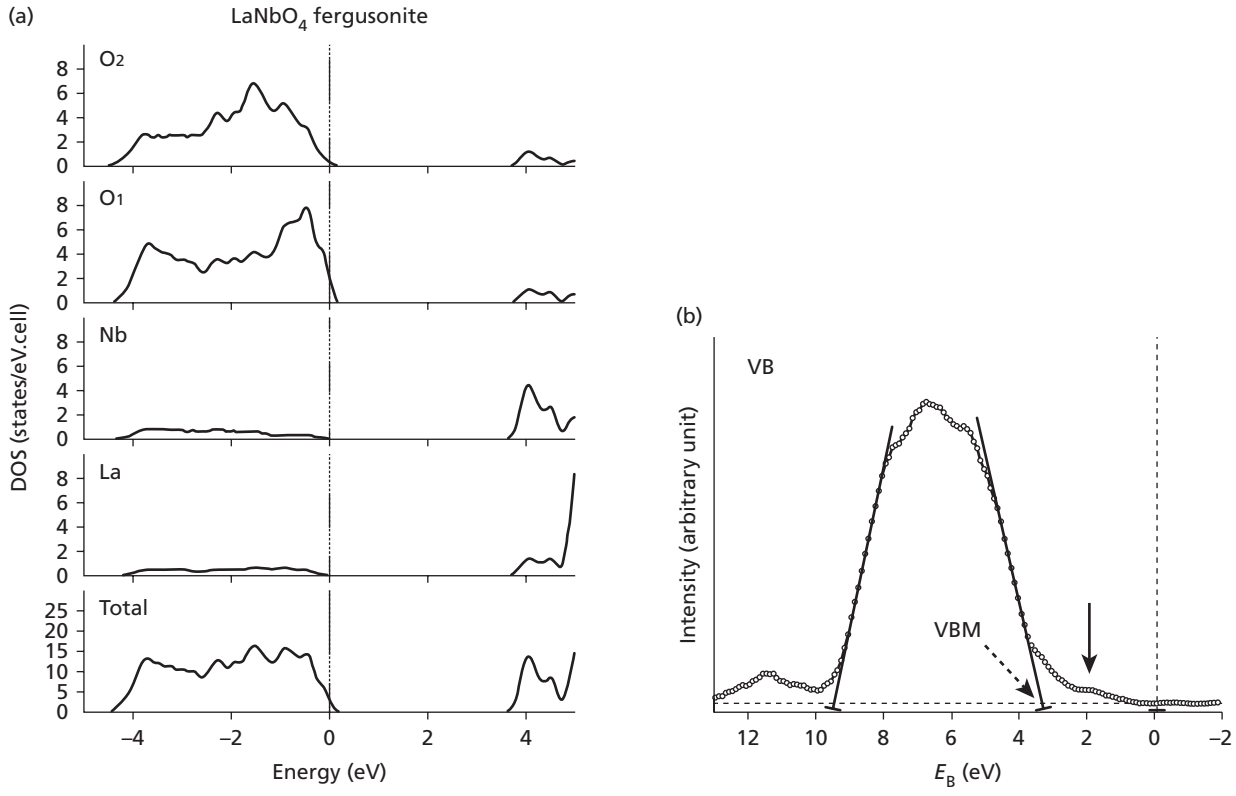

Figure 5. (a) DOSs calculated for $LaNbO_4$ with the fergusonite crystal structure. The DOSs were broadened with the Gaussian function of full width at half maximum of 0·1 eV for convenience of comparison with the experimental VB spectrum. (b) VB spectrum of the $La(Nb_{0·75}V_{0·04}Mn_{0·21})O_4$ sample. The bold arrow at ≈2 eV indicates the occupied states generated by Mn^{4+} substitution for the V^{5+} sites. The hump around E_B ≈11·5 eV is due to the adventitious carbon. DOS, density of states; VB, valence band.

O_1 and the last is in common for O_1 and O_2. The calculated band gap (E_g) amounted to 3·5 eV. However, it is known that GGA generally underestimates E_g. Here, we note that no state in E_g is seen in the calculated DOS. The partial DOSs of the conduction bands indicated that the dominant contributions are from La and Nb. The partial DOS of Nb 4*d* distributed in a relatively lower energy region than that of La 5*d*. Figure 5(b) shows the experimental VB spectrum with the onset at E_B ≈3 eV and the width of ≈6 eV of the $La(Nb_{0·71}V_{0·04}Mn_{0·25})O_4$ sample. The bumpy spectrum mainly consisted of three components, which indicate the O 2*p* states reflected inequivalent oxygen sites due to the fergusonite crystal structure. A small hump centered at ≈2 eV appeared additionally. When the onset at ≈3 eV corresponds to the calculated VBM, the occupied states around 2 eV correspond to the occupied state in E_g generated by Mn^{4+} substitution for the V^{5+} sites.

4. Conclusions

The authors synthesized $La(NbVMn)O_4$ samples with the composition of La:Nb:V:Mn = 1:0·71:0·04:0·25, and the fergusonite crystal structure is isostructural to the ferroelastic $LaNbO_4$. XPS clarified the La^{3+}, Nb^{5+}, V^{5+} and Mn^{4+} chemical states for the $La(Nb_{0·71}V_{0·04}Mn_{0·25})O_4$ samples. Mn^{4+} substituted for the V^{5+} sites and resulted in FM behavior in *M-T* with the Curie temperature of ≈200 K and sigmoidal *M-H* curve with $M = 3\ \mu_B$ at 75 K and 1 T. The observed FM behavior is originated from growth in distance of exchange interactions between dispersed $Mn^{4+}Nb_2O_{11}$ nanoclusters. The $La(NbVMn)O_4$ is promising not only for the development of nanoscale stress-switchable information storage material at low temperatures but also for the high proton conductivity at high temperature due to Mn^{4+} substitution for the V^{5+} sites.

Acknowledgements

The study was partly supported by the "Nanotechnology Support Project" of the Ministry of Education, Culture, Sports, Science and Technology, Japan, and the inter-university cooperative research program of (Proposal No. 11G0003) the Cooperative Research and Development Center for Advanced Materials, Institute for materials Research, Tohoku University.

REFERENCES

1. Baek, S. H.; Jang, H. W.; Folkman, C. M.; Li, Y. L.; Winchester, B.; Zhang, J. X.; He, Q.; Chu, Y. H.; Nelson, C. T.; Rzchowski, M. S.; Pan, X. Q.; Ramesh, R.; Chen, L. Q.; Eom, C. B. Ferroelastic switching for nanoscale non-volatile magnetoelectric devices. *Nature Mater* **2010**, *9*, 309.
2. Virkar, A. V.; Jue, J. F.; Smith, P.; Metha, K.; Prettyman, K. The role of ferroelasticity in toughening of brittle materials. *Phase Transitions* **1991**, *35*, 27.
3. Blasse, G.; Brixner, L. H. Ultraviolet emission from ABO_4-type niobates, tantalates and tungstates. *Chemical Physics Letters* **1977**, *38*, 55.
4. Hsiao, Y. J.; Fang, T. H.; Chang, Y. S.; Chang, Y. H.; Liu, C. H.; Ji, L. W.; Jywe, W. Y. Structure and luminescent properties of $LaNbO_4$ synthesized by sol–gel process. *Journal of Luminescence* **2007**, *126*, 866.
5. Arai, M.; Wang, Y. X.; Kohiki, S.; Matsuo, M.; Shimooka, H.; Shishido, T.; Oku, M. Dielectric property and electronic structure of $LaNbO_4$. *Japanese Journal of Applied Physics* **2005**, *44*, 6596.
6. Kim, D.-W.; Kwon, D.-K.; Yoon, S. H.; Hong, K. S. Microwave dielectric properties of rare-earth ortho-niobates with ferroelasticity. *Journal of the American Ceramic Society* **2006**, *89*, 3861.
7. Haugsrud, R.; Norby, T. Proton conduction in rare-earth ortho-niobates and ortho-tantalates. *Nature Materials* **2006**, *5*, 193.
8. Haugsrud, R.; Norby, T. High-temperature proton conductivity in acceptor-doped $LaNbO_4$. *Solid State Ionics* **2006**, *177*, 1129.
9. Takei, H.; Tsunekawa, S. Growth and properties of $LaNbO_4$ and $NdNbO_4$ single crystals. *Journal of Crystal Growth* **1977**, *38*, 55.
10. Brik, F.; Enjalbert, R.; Galy, J. Synthese, cristallisation et determination structurale d'un compose de type scheelite dans le systeme lanthane-niobium-vanadium-oxygene. *Materials Research Bulletin* **1994**, *29*, 15.
11. Jia, Y. Q. Crystal radii and effective ionic radii of the rare earth ions. *Journal of Solid State Chemistry* **1991**, *95*, 184.
12. Mather, G. C.; Fisher, C. A. J.; Islam, M. S. Defects, dopants, and protons in $LaNbO_4$. *Chemistry of Materials* **2010**, *22*, 5912.
13. Kuwabara, A.; Haugsrud, R.; Stlen, S.; Norby, T. Local condensation of oxygen vacancies in t-$LaNbO_4$ from first principle calculation. *Physical Chemistry Chemical Physics* **2009**, *11*, 5550.
14. Wagner, C. D.; Riggs, W. M.; Davis, L. E.; Moulder, J. F.; Muilenberg, G. E. (eds.) *Handbook of X-Ray Photoelectron Spectroscopy*. Minnesota: Perkin-Elmer, 1979.
15. Blaha, P.; Schwartz, K.; Madsen, G. K. H.; Kvasnicka, D.; Luitz, J. *WIEN2k, An Augmented Plane Wave + Local Orbitals Program for Calculating Crystal Properties*. Vienna: Vienna University of Technology, 2001.